Investigation of Passive Flow Control of Cavity Acoustics Using Dynamic Pressure-Sensitive Paint

Jim Crafton[1], Scott Stanfield[2], Nikolay Rogoshchenkov[3]
Innovative Scientific Solutions, Inc., Dayton, Ohio

Ryan Schmit[4]
Air Force Research Laboratory, Wright-Patterson AFB, Ohio

Spatially resolved pressure fluctuations were measured on the ceiling of a rectangular cavity using pressure-sensitive paint for the frequency range of 100 to 5000 Hz. The measurements were acquired at Mach 0.7 and 1.5 for a clean cavity, and with four different flow control devices placed at the leading edge of the cavity. The high spatial resolution of the PSP data allowed the pressure waves to be visualized as they moved down the cavity. Time-resolved pressure data was analyzed to reveal frequency spectrum, identify Rossiter tones, and compute sound pressure levels in the cavity. The frequency and amplitude of the PSP data were in good agreement with conventional dynamic pressure sensors that were located along the length of the cavity centerline. Comparisons of the PSP spectral data with the pressure transducer spectral data indicate a noise floor for the PSP data of about 105-dB for the supersonic data. The high spatial resolution spectral maps indicated asymmetric structure in the higher order Rossiter tones with several of the flow control devices. Analysis of the data using Proper Orthogonal Decomposition revealed that the asymmetric structure was present, but very weak, in the baseline case. This suggests that the flow control devices were not creating the asymmetry, but enhancing an already present structure. This asymmetry was not evident in the subsonic data.

I.Nomenclature

CMOS	=	complementary metal-oxide semiconductor
LED	=	light emitting diode
POD	=	proper-orthogonal decomposition
PSP	=	pressure-sensitive paint
SPL	=	sound pressure level

I. Introduction

CAVITIES such as landing gear bays and weapon bays generate flowfields with high-intensity acoustic signatures. The nature of the acoustic signal can be entirely broadband noise in the case of a closed cavity or, in the case of an open cavity, a superposition of broadband noise and discrete tones known as Rossiter modes.[1] In general, the broadband acoustics of a closed cavity complicates the release of stores, and while this concern is greatly reduced for open cavities, the frequencies and amplitudes of the Rossiter modes can cause significant structural damage. Relocating stores underneath wings eliminates the inherent complexity of internal storage at the cost of added drag and elevated noise levels that are detrimental to stealth. For these reasons, the reduction of the acoustic levels of Rossiter tones for open cavity configurations in recent years has been the subject of many experimental and

---

[1] Vice President, Innovative Scientific Solutions Inc., Senior Member AIAA
[2] Research Scientist, Innovative Scientific Solutions Inc.
[3] Research Scientist, Innovative Scientific Solutions Inc.
[4] Principal Aerospace Engineer, Air Force Research Laboratory

computational studies involving active and passive flow control devises. In this paper, fast pressure-sensitive paint was utilized to spatially resolve the pressure fluctuations on the cavity ceiling of an open cavity with an aspect ratio, *L*/*D*, of 5.67. Four different passive flow control devices were placed at the leading edge of the cavity and the resultant fluctuating pressure field was compared with a rectangular cavity to determine the effects of each flow control devise. The flow control devises investigated included a rod, ridges, steps, and flat spoiler. The Mach number for all results presented within this paper was 0.7 and 1.5.

In open cavities, the freestream flow separates at the leading edge of the cavity, forms a shear layer between the freestream and cavity flows, and impinges on the aft wall of the cavity. The interaction of the impinging shear layer with the aft wall causes the development of the high intensity Rossiter modes which propagate upstream in the cavity and interact with the separation of the flow at the leading edge, creating a closed loop. The frequency of the Rossiter tones at Mach 0.7 is given as

$$f_m = \frac{U_\infty}{L}\left[\frac{m-\alpha}{M_\infty + 1/k_v}\right] \tag{1}$$

and at Mach 1.5 as

$$f_m = \frac{U_\infty}{L}\left[\frac{m-\alpha}{M_\infty\left\{1+\frac{(\gamma-1)M_\infty^2}{2}\right\}^{-1/2} + 1/k_v}\right] \tag{2}$$

In Equations 1 and 2, U_∞ is the freestream velocity, *M* is the Mach number, *L* is the cavity length, *m* is the integer mode number, *k* is the ratio of the convective velocity of the vortices in the shear layer to the freestream velocity, and γ is the phase delay between the impact of the acoustic wave at the cavity front wall and the formation of the new vortex.[2]

In addition to the Rossiter tones, the flow in an open cavity circulates resulting in a nearly uniform static pressure distribution on the cavity ceiling with a slight increase toward the downstream wall which significantly differs from the nonuniform distribution of the fluctuating pressure component.[2] Hence, several point sensors distributed along the cavity ceiling is sufficient to resolve the mean surface pressure but doesn't adequately describe the distributed loading created by the Rossiter modes. To properly evaluate flow control devises for open cavities, the fluctuating pressure should be resolved spatially and temporally. This was one of the reasons a fast-responding pressure-sensitive paint (PSP) was utilized for the work presented.

The fast PSP selected for the work presented responds to acoustic disturbances up to at least 20,000 Hz. The sample rate and record length used resulted in a frequency range from 100 to 5,000 Hz. Unfortunately, the frequency content of the fluctuating surface pressure at frequencies greater than 5,000 Hz was not insignificant, and the data collected is aliased. The sample rate could have been increased to eliminate aliasing but the cost in signal would have been too much. A better approach recently implemented by ISSI is to tailor the paint chemistry to achieve the desired frequency response. This allows for an optimal selection of the exposure time or frame rate, signal levels, and frequency response. As will be shown, the contributions from aliasing was significantly lower than the sound pressure levels of the Rossiter tones. Hence, useful information can still be determined from the data collected at the frequencies corresponding to the Rossiter tones.

II. Experimental Approach

Pressure-Sensitive Paint[3] (PSP) offers non-intrusive pressure measurements with high spatial resolution; however, the response times of standard paints are on the order of one second. Fast responding PSP formulations for dynamic pressure measurements have been developed[4] and demonstrated[5]. These formulations include anodized aluminum and porous polymer paints that have demonstrated bandwidths of up to 100 kHz (i.e., response times of ~10 μs). Over the past few years, ultra-bright LEDs and fast-framing CMOS (complementary metal-oxide semiconductor) cameras have been developed that have significantly improved the performance of fast PSP systems. Fast responding PSPs combined with fast framing digital cameras and ultra-bright illumination sources have been used to produce systems that acquire millions of data points at speeds of several kHz. The resulting system acts as an array of fast pressure transducers and the resulting data can be analyzed to provide frequency content of the flow at each spatial location. Dynamic PSP systems have been used to identify structures in cavity flows[6], study shock boundary layer interactions[7], and investigate transverse jet injection in supersonic flows[8].

A. Experimental Setup

Experiments were conducted at the Trisonic Gasdynamics Facility (TGF), located on Area B of Wright-Patterson Air Force Base. The closed circuit wind tunnel can achieve subsonic velocities from Mach 0.23 to 0.87, and discrete supersonic Mach numbers of 1.5, 1.9, 2.3 and 3.0 with interchangeable nozzle blocks. The test section is 607 mm high, 607 mm wide and 1219 mm long. Two 660 mm diameter flat windows on either side of the test section provide optical access to the flow and model. The primary model support is a crescent mounted sting, which can be used to reach various attitudes or model orientations, including pitch from -1° to +18.5°, and roll from -90° to +180°. The current experiments were conducted at Mach 0.7 and 1.5 with corresponding unit Reynolds numbers of 6.6×10^6/m and 7.5×10^6/m while the stagnation temperature was held constant at 300 K.

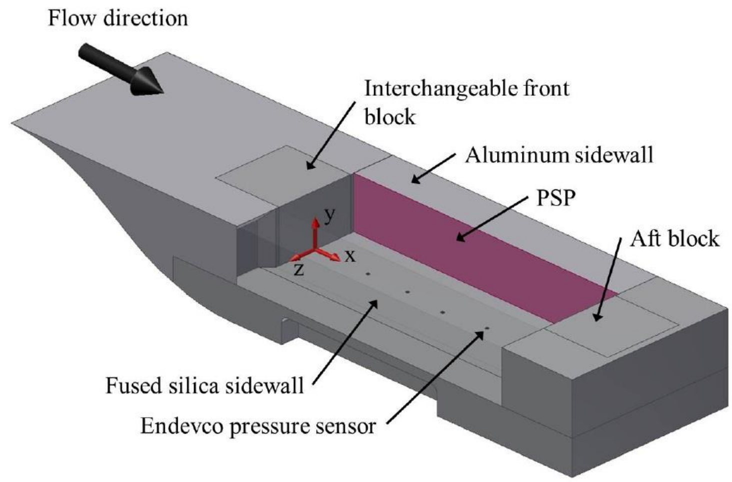

Figure 1. Schematic of optical turbulence reduction cavity model.

The new Optical Turbulence Reduction Cavity model was built and has been used in several previous investigations.[9,10,11] With three interchangeable optical-quality fused silica windows that serve as the cavity ceiling and two side walls, this model provides unique optical access to inside the entire cavity. The windows are replaceable with aluminum blanks, and for the current investigation, the cavity configuration utilized aluminum side walls. The cavity ceiling window was an aluminum blank that contained two thermocouples, five static pressure ports and seven Endevco dynamic pressure sensors. All sensors were located along the cavity center line. The dynamic pressure sensors, numbered 1 to 7, were located 10.8, 43.18, 75.57, 107.95, 140.34, 172.72, and 205.11 mm downstream of the cavity leading edge.

Figure 1 shows a schematic of the cavity model highlighting some of its major features. The dimensions of the cavity were 216 mm long, 38 mm deep, and 63.5 mm wide (L/D = 5.67). The fore body of the model was 178 mm long and 127 mm wide. The front and aft wall blocks of the cavity were designed to be replaceable so that both passive and active flow control devices can be examined. For the current investigations, only the forward wall block was interchanged with different passive flow control devices. The aft wall block was rectangular. To ensure an attached boundary layer along the fore body of the cavity, the pitch angle was set to -0.75°.

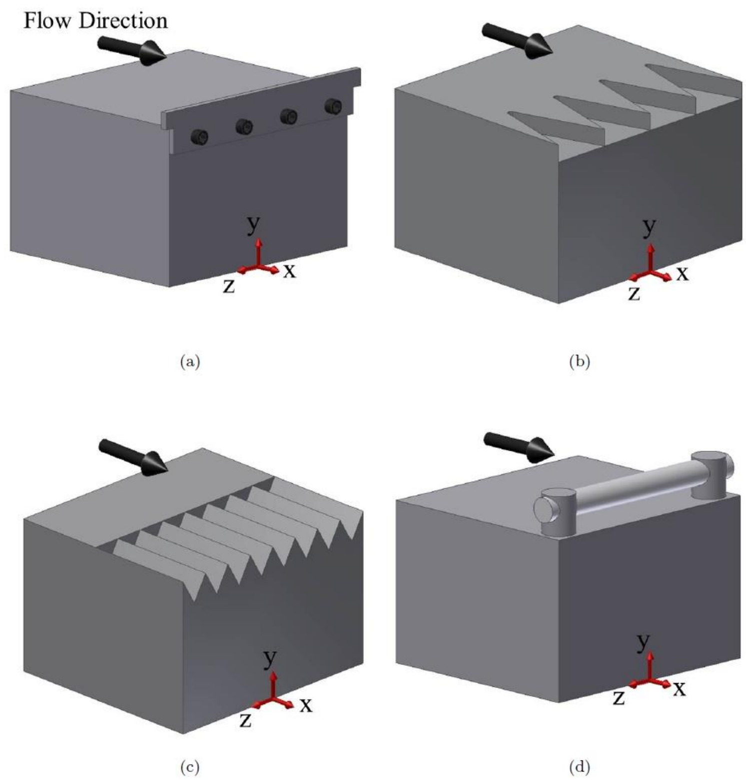

Figure 2. Flow control devices: (a) flat spoiler, (b) triangular steps, (c) ridges, and (d) cylindrical rod.

The baseline case used rectangular front and aft blocks to create a conventional cavity geometry. Four different passive flow control devices which altered the geometry of the cavity's leading edge were also investigated. The passive devices examined were a flat spoiler, a series of triangular backward-facing steps, ridges, and a horizontal rod in cross flow. Descriptions of the flow control devises used in this study can be found in Schmit et al.[9] A schematic of each device are shown in Figure 2. The flat spoiler (Figure 2 (a)) was 63.5 mm wide, spanning the width of the cavity, protruded 4.0 mm above the cavity waterline, and was 1.6 mm thick. The protruding spoiler acts to lift the separating boundary layer, which reduces impingement of the shear layer on the rear wall, thereby altering the cavity wave dynamics and sound pressure levels. The triangular steps (Figure 2 (b)) were comprised of four triangular-shaped cutouts with a maximum depth of 4.0 mm that extended 25.4 mm upstream from the cavity's leading edge. The ridges flow control device (Figure 2 (c)) consisted of eight V-shaped, streamwise grooves. The grooves were 6.4 mm deep, 25.4 mm long, and have a 60° interior angle. Both the large triangular steps and ridges are thought to induce streamwise vorticity into the shear layer. The final flow control device was a horizontal rod (Figure 2 (d)). The 63.5 mm wide, 6 mm diameter ceramic rod was held in position by two 8 mm diameter posts. The gap spacing between the rod and cavity waterline was set to 2.54 mm. Vortex shedding from the rod is thought to break up the large coherent structures in the cavity shear layer.

B. Unsteady Pressure-Sensitive Paint

PSP is an image-based technology that has been used for continuous measurements of pressure on aerodynamic surfaces. The paints are composed of a pressure sensitive dye in a polymer binder and paint application is performed using a spray can or airbrush. The measurement is accomplished by applying the paint to the surface of interest and illuminating the surface with blue or UV light to excite the dye. The surface is imaged through a filter that isolates the excitation light from the pressure sensitive luminescence of the paint. Each pixel on the camera then acts as a pressure tap, and therefore, continuous distributions of the pressure on the painted surface are acquired. Standard pressure paints can be used for mean measurements with response times of about 1-Hz and fast response[12] systems can be used for high frequency measurements, with a bandwidth of over 100-kHz.

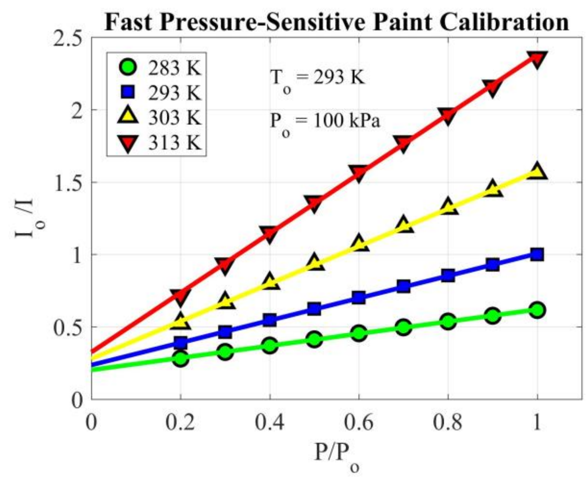

Figure 3: Calibration of PtTFPP-PP fast response PSP.

The use of standard PSP is becoming more common in large transonic tunnels, with production systems in use in several facilities such as TsAGI[13], AEDC[14], DLR[15], and ARA[16]. Fast responding PSP offers a means of acquiring unsteady pressure data at millions of locations on a model surface. This is accomplished by combining a fast-responding PSP with a fast framing CMOS camera and an ultra-bright LED. Fast responding PSP formulations based on polymer/ceramic, a formulation first demonstrated by Scroggin[17], have been used to demonstrate the potential of fast PSP in several wind tunnels over the last 5 years. The calibration of the fast PSP formulations used in this work, ISSI PP-Fast PSP, is shown in Figure 3. Note that while PtTFPP-PP is very fast (~20 kHz), it is also very temperature sensitive.

C. Unsteady Pressure-Sensitive Paint Data Processing

The standard radiometric PSP data processing scheme involves the computation of the wind-off to wind-on ratio and then the conversion of this ratio to pressure. This traditional radiometric approach is susceptible to several sources of error, particularly model motion. The key to processing dynamic PSP data is to recognize that many of the traditional radiometric error sources are DC errors. For example, variations in model temperature, photo-degradation of the paint, and sedimentation occur at low temporal frequencies. A significant portion of the model motion occurs between the wind-off and wind-on image, with minor model vibration occurring at 10s of Hz. To mitigate these issues, ISSI has implemented an AC coupled data processing scheme.

The first step in fast PSP data processing is to align the wind-on images and compute the average. This average wind-on is then used as the reference image for subsequent data processing. The average wind-on is then divided by each individual wind-on image, and the resulting ratio is converted to pressure using the slope of the PSP calibration. The raw images from the cavity test were converted to pressure for each model configuration at the subsonic and supersonic conditions listed in Section A. The data was low-pass filtered and mapped from the bitmap to a surface mesh of the cavity ceiling (1024 by 400 bitmap to 108 by 32 mesh). The mesh represents the surface of the cavity ceiling in physical space with a spatial resolution of 2 mm.

D. Unsteady Pressure-Sensitive Paint Data Analysis

Simply acquiring unsteady pressure maps is only the first step in exploiting the capabilities of dynamic PSP. Current PSP data analysis techniques are not suitable for analyzing these extremely large and often complex data sets. Tools that allow the user to quickly decompose the data and identify key flow features or spectral content are essential for effective use of dynamic PSP. Examples of these tools include simple correlation analysis[18], spectral analysis[19], proper orthogonal decomposition (POD)[20], and dynamic mode decomposition (DMD)[21]. Each of these tools has been demonstrated with dynamic PSP data and each has shown the capacity to reveal key insights into specific flows as well as isolate various noise sources. The reader is directed to the above references for more detailed description of the data processing tools. The key tools used to analyze the current data set are spectral analysis and POD. A short overview of these techniques is included in the following.

Once the entire record length had been binned, calibrated, and scaled, the sound pressure level (SPL) at each frequency was determined. The SPL is defined as

$$SPL = 20\log\left(\frac{RMS}{P_0}\right) \tag{3}$$

where *RMS* is the root mean square pressure, and P_0 is a reference pressure of 20 µPa. For the purpose of the work presented, Equation 3 is given below in terms of the autospectral density function, *G*.

$$SPL = 10\log\left(\frac{RMS}{P_0}\right)^2 \tag{4}$$

$$SSPL = 10\log\left(\frac{Var}{P_0^2}\right) \tag{5}$$

$$SPL(f) = 10\log\left(\frac{G(f)}{P_0^2}\right) \tag{6}$$

The power spectral density and sound pressure level at a set of points on the model yield important insight into the frequency content of a given time series. This technique, however, only provides an understanding of the spatio-temporal nature of the dynamics of the entire system. In unsteady, turbulent flows, POD provides for the extraction of relevant flow structures that present a characteristic temporal life cycle, as well as the frequency content of those flow features. POD analysis has also lent itself for use as a filter of spurious data and noise in particle image velocimetry. Recently, POD analysis was applied to unsteady PSP data from a cavity acoustics test in a large wind tunnel test by Sellers[22] with promising results.

The POD technique seeks to represent a high-dimensional pressure field with a low-dimensional model, characterized by the summation of mode shapes, or basis functions:

$$p(x,t) = \sum a_n(t)\varphi_n(x) \tag{7}$$

In Equation 7, *x* represents a spatial coordinate and *t* a time coordinate. The pressure, *p*, is approximated by the summation of the product of a time constant, a_n, and a spatial POD mode, φ_n for a discrete set of data. The modes are orthogonal and are ordered based on turbulent kinetic energy. For modal decomposition, the "snapshot" method is used, having obtained a set of *N* spatial- and time-resolved data for regions where the model was painted. For each instant in time, a column vector of the fluctuating pressure at *M* grid points is organized, which collectively form an *M* x *N* matrix, *U*. A correlation matrix is created by multiplying the *U* matrix with its transpose. Then an eigenvalue problem is set up based on Equation 8, where A^i is the matrix of eigenvectors and λ^i are the eigenvalues. The solution is organized from largest to smallest eigenvalue, with $\lambda^N = 0$. Finally, the eigenvectors are used to calculate the POD modes using Equation 9.

$$\tilde{C}A^i = \lambda^i A^i \tag{8}$$

$$\varphi^i = \frac{\sum_{n=1}^{N} A_n^i u^n}{\left\| \sum_{n=1}^{N} A_n^i u^n \right\|} \quad i = 1, \cdots, N \tag{9}$$

After being decomposed into N modes, the instantaneous pressure field can be reconstructed using Equation 7, where the time constant, a_n, can be calculated according to the following equation:

$$a_n(t) = diag\left(\sqrt{\lambda_n}\right) A_n^{\mathrm{T}} \tag{10}$$

Typically, the predominant flow features in the cavity are found in the first few POD modes. It is important to determine how many modes are relevant for analysis and how many modes should be used for reconstructing pressure fields.

III.Results

Data analysis included conversion of each PSP image to pressure, computation of pressure fluctuations, spectral maps, POD modes, reconstruction of the data using POD modes, and computation of the spectral content using the reconstructed pressure data. This analysis was performed for both the Mach 1.5 and 0.7 data sets with the baseline cavity and each of the flow control devices.

A. Unsteady PSP Data and Pressure Fluctuations

A total of 30,000 to 62,000 images were acquired at five test configurations (baseline plus four flow control setups) at Mach numbers of 0.7 and 1.5. The sample rate for the PSP data was 10,000 Hz at Mach 1.5 and 5,000 Hz at Mach 0.7. Wind-off and background data was also acquired at each test condition and the data was processed and mapped onto the 108 by 32 mesh as described previously. Seven Endevco pressure transducers were mounted flush with the cavity ceiling along the length of the centerline at x = 10.80, 43.18, 75.57, 107.95, 140.34, 172.72, and 205.11 mm, with the origin at the cavity leading edge. Data was acquired from the pressure transducers at 75-khz at each test condition, unfortunately, the data was not synchronized with the PSP data acquisition.

A progression of PSP images taken over 800-μs at Mach 1.5 with no flow control device attached to the model is presented in Figure 4. The images show a succession of pressure wave traveling downstream in the cavity and reflecting from the back wall. Multiple waves are visualized in several of the images. While several of the pressure waves are

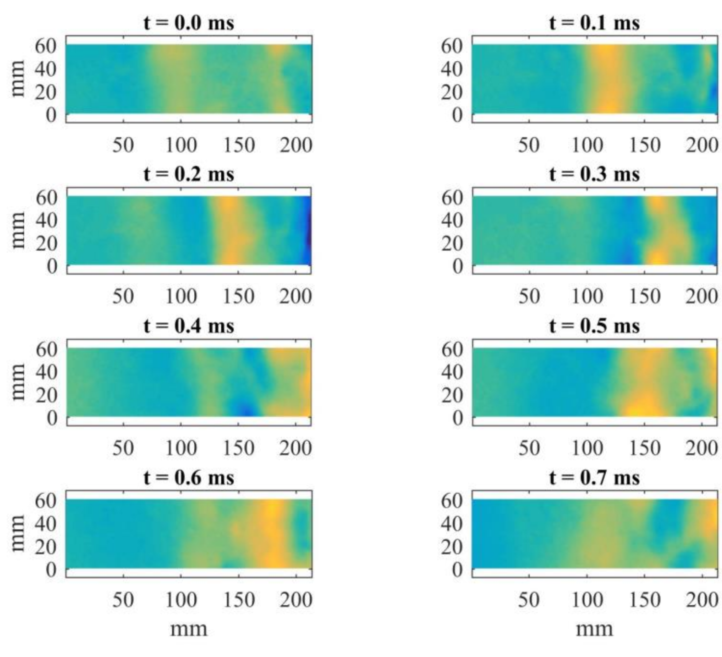

Figure 4: PSP results over 800 μs with no flow control (flow is left to right).

somewhat planer, there is some two-dimensional structure to several of the waves on the cavity floor. The scale of the colormap in Figure 4 is +/- 10 kPa, and therefore, the amplitude of these pressure waves is on the order of 10 kPa.

The time history of the pressure data can be extracted at each pixel and quantitates such as the amplitude of the pressure fluctuations and spectral content of the flow at each pixel can be computed. A map showing the amplitude of the pressure fluctuations at each pixel in the cavity is shown in Figure 5. The amplitude of the pressure fluctuations increases from the front of the cavity to back of the cavity. The pattern is generally planar, with some curvature near the corners at the back of the cavity.

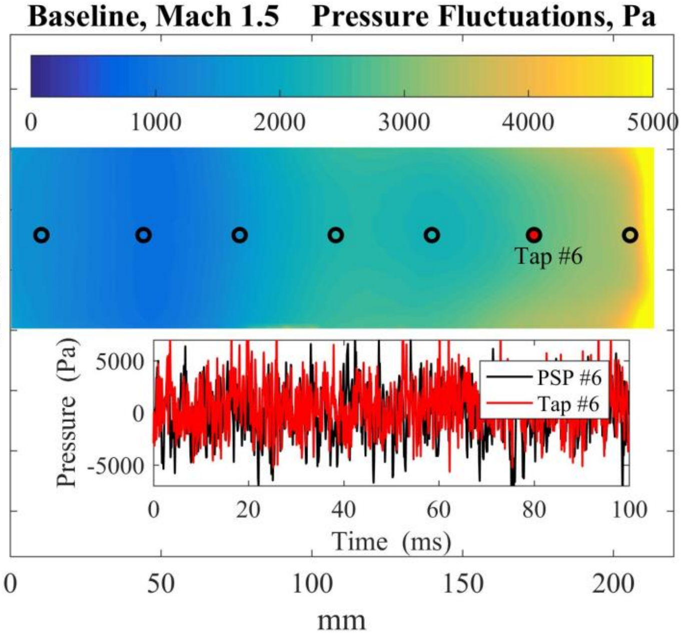

Figure 5: Map of fluctuating pressure for the Mach 1.5 Baseline cavity configuration. (Note that PSP and Tap data was not sampled simultaneously)

The PSP data was extracted near each pressure tap and the data from the PSP and tap at location six is also shown in the figure. The amplitude of the pressure fluctuations from the PSP and pressure tap were 2693 Pa and 2330 Pa respectively. The PSP data generally indicated a level of pressure fluctuations about 300 Pa higher than the comparable tap at each location. An analysis of the shot noise for a single PSP image results in a noise floor of about 250 Pa for the fluctuating pressure measurement, and therefore, it is possible that shot noise contributed to this disagreement between the taps and PSP. It is also possible that low frequency model vibration, which would manifest as a low frequency pressure fluctuation in the PSP data, may have contributed to this slightly higher fluctuationg pressure from the PSP data.

B. Spectral Content of the Flow

The power spectrum of the time resolved pressure data was computed at each pixel and converted to sound pressure level (SPL) resulting in a series of maps that show the amplitude of the pressure fluctuations in each frequency bin. To quickly identify key frequencies in the cavity, the mean amplitude of the spectra at each frequency was extracted and organized from largest to smallest. The frequency of the Rossiter modes is listed in Table 1. This data indicated that the second Rossiter mode was the dominate feature, and therefore, the spectral map at this frequency is shown in Figure 6.

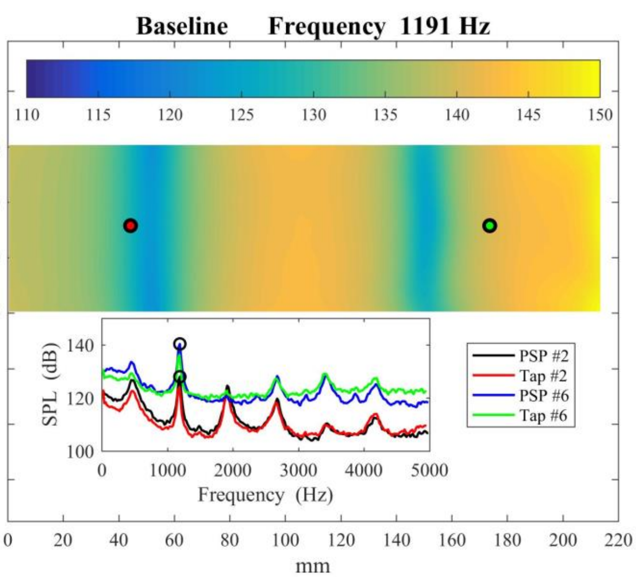

Figure 6: Map of fluctuating pressure at 2^{ond} Rossiter tone for the Mach 1.5 Baseline cavity configuration.

The planar structure of the cavity tone is evident in the figure, with two cancelation nodes surrounded by much larger amplitude peaks. The SPL is greatest at the back wall of the cavity, as was the case for the pressure fluctuation map, for all tones and reaches a maximum value of 154 dB for the second Rossiter mode. The spectral content at two of the seven tap locations were compared and displayed at the bottom of Figure 6. Note that the PSP and tap data is in near perfect agreement at each of the Rossiter tone frequencies, and the amplitude of each peak is within 4.4 dB in the worst case (Tap 2 at tone 1). This level of agreement in the amplitude data is equal to about 17 Pa in fluctuating pressure amplitude. It is noted that this is lower than the single image shot noise computed previously. This apparent improvement in the resolution of the PSP data is a result of signal averaging in the spectral computation where the spectrum was computed using 512 points but the record length was 30,000 points.

Table 1: Peak Rossiter frequencies from the side wall and ceiling tests at Mach 1.5.

Mode	Side Wall (Hz)	Ceiling (Hz)
1	502	462
2	1187	1194
3	1938	1914
4	2673	2658
5	3494	3429
6	4177	4161

The frequency content of the flow was computed for the baseline and each flow control condition using the sequence of pressure images. SPL contours of the cavity ceiling at the first, second, third, fourth, fifth, and sixth Rossiter modes for the baseline, rod, flat spoiler, ridges, and triangular step inserts are shown in Figure 7 - Figure 12, respectively. For the baseline configuration, the SPL contours are close to symmetric about the cavity centerline. Of the four flow control devices, the rod in cross flow suppresses pressure fluctuations most effectively while the triangular step is slightly less effective. The flat spoiler and ridges show poor suppression compared to the baseline flow. The most obvious feature in the SPL contours is the strong asymmetric distribution of the pressure peaks generated by the flat spoiler. This feature is present at each frequency, but is most pronounced at the second tone. This asymmetric distribution is also present at each tone for the rod in crossflow. The SPL was lowered by approximately 30 dB at the back wall of the cavity by the rod in crossflow while the flat spoiler performance was slightly worse than the baseline case. Clearly the asymmetric distribution is not key to the cavity acoustics. The typical periodic structure in the SPL on the cavity ceiling is still present with the rod in cross flow, but is significantly mitigated. This may be indicative of the rod in crossflow breaking up the coherent structures that set up the Rossiter tones.

The line profiles along the cavity length at y = 14 mm for the first, second, third, and fourth Rossiter tones are shown in Figure 13. The modal nature of the Rossiter tones is evident in the local minima observed in the profiles. For the first Rossiter tone, there is a single local minimum around x = 90 mm. The location of this saddle point depends on the flow control devise inserted. For the triangular steps, the location of the minimum is significantly shifted to x = 45 mm. The location of the minimum points for the second Rossiter tone also shift somewhat, but are similar to the baseline configuration. As already noted, the SPL profile for the cylinder does not show strong Rossiter modes, they are however distinguishable. Finally, the modes are weak for the triangular step insert but again, are still present.

C. Proper Orthogonal Decomposition

The baseline cavity pressure data at Mach 1.5 was decomposed using the POD technique. The data was processed using 8,192 of the 30,000 images resulting in the computation of 8,192 modes. Typically, the predominant features are found in the first few POD modes. As an example, the distribution of energy in each mode is plotted in the top left corner of Figure 14. Approximately 40% of the energy is in the first mode, with the second, third, and fourth modes containing 18%, 14%, and 7% of the energy respectively. Over 90% of the energy is contained in the first 11 modes, and 99% of the energy is in the first 79 modes. The structure of the first 11 modes is displayed in Figure 14 - Figure 15. Note that modes 1 through 6 and mode 10 have a planar pattern and spatial distribution similar to the Rossiter tones found in the baseline cavity configuration in Figure 7 - Figure 12. This result is anticipated as there is significant energy in the pressure fluctuations at the Rossiter tones.

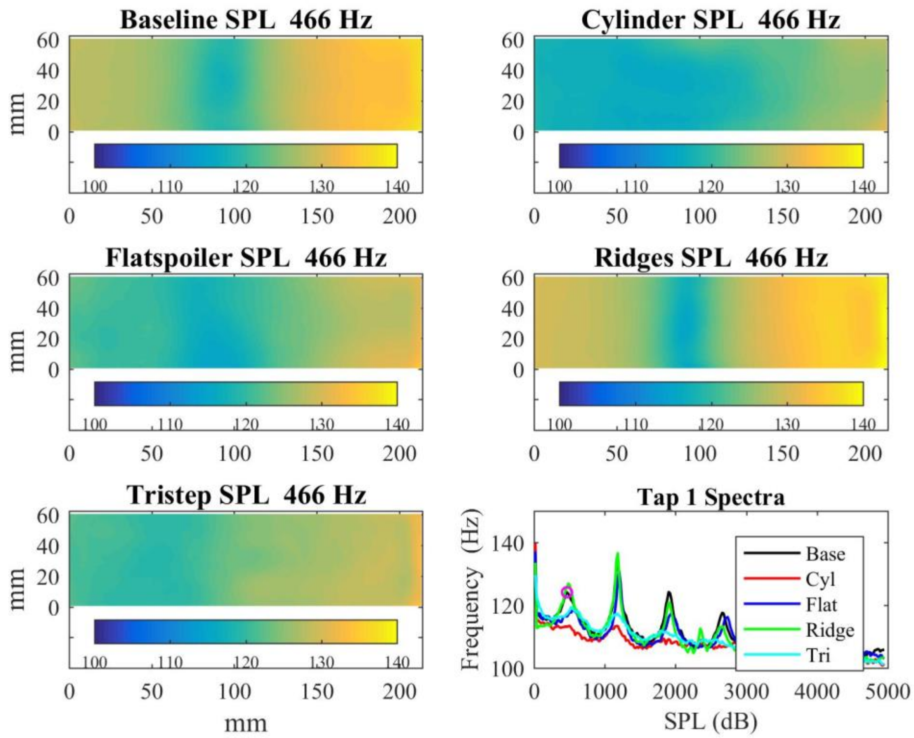

Figure 7. SPL contours for baseline and all control cases at M = 1.5 for the 1st Rossiter tone.

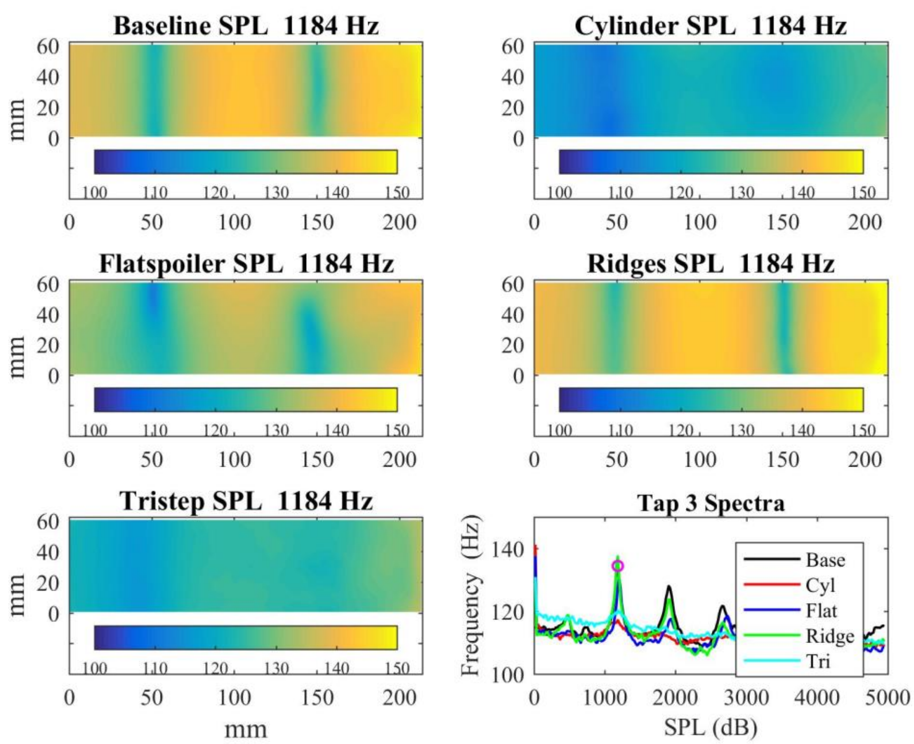

Figure 8. SPL contours for baseline and all control cases at M = 1.5 for the 2nd Rossiter tone.

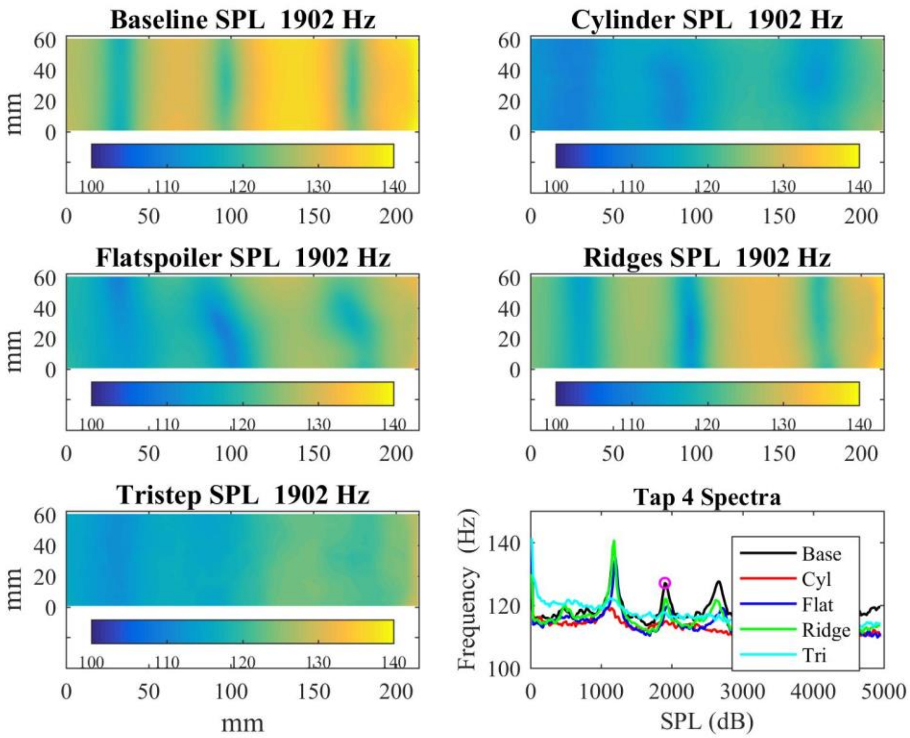

Figure 9. SPL contours for baseline and all control cases at M = 1.5 for the 3rd Rossiter tone.

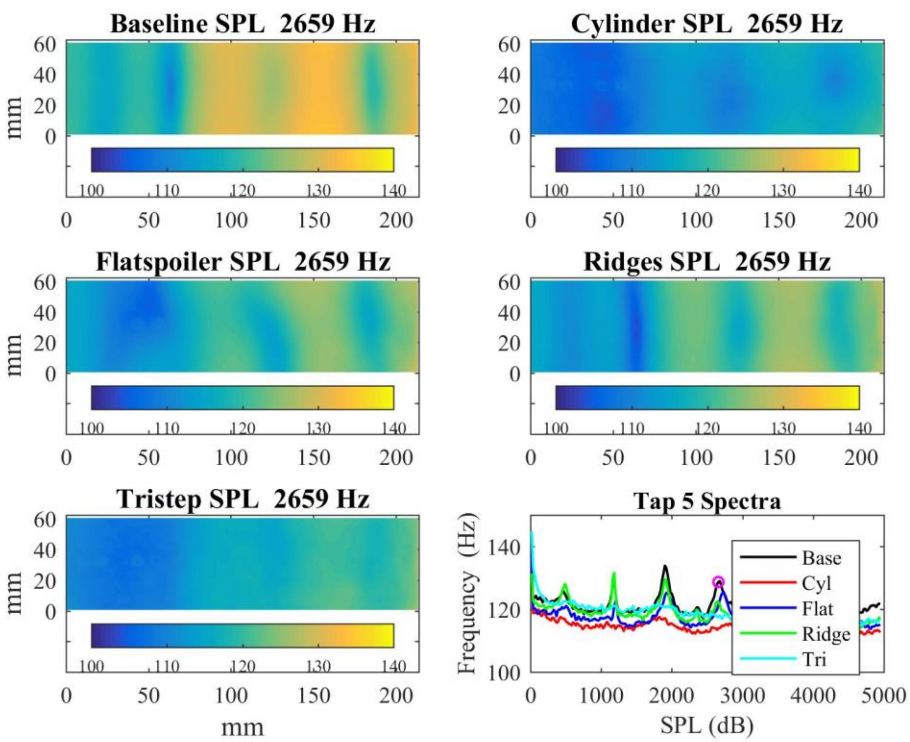

Figure 10. SPL contours for baseline and all control cases at M = 1.5 for the 4th Rossiter tone.

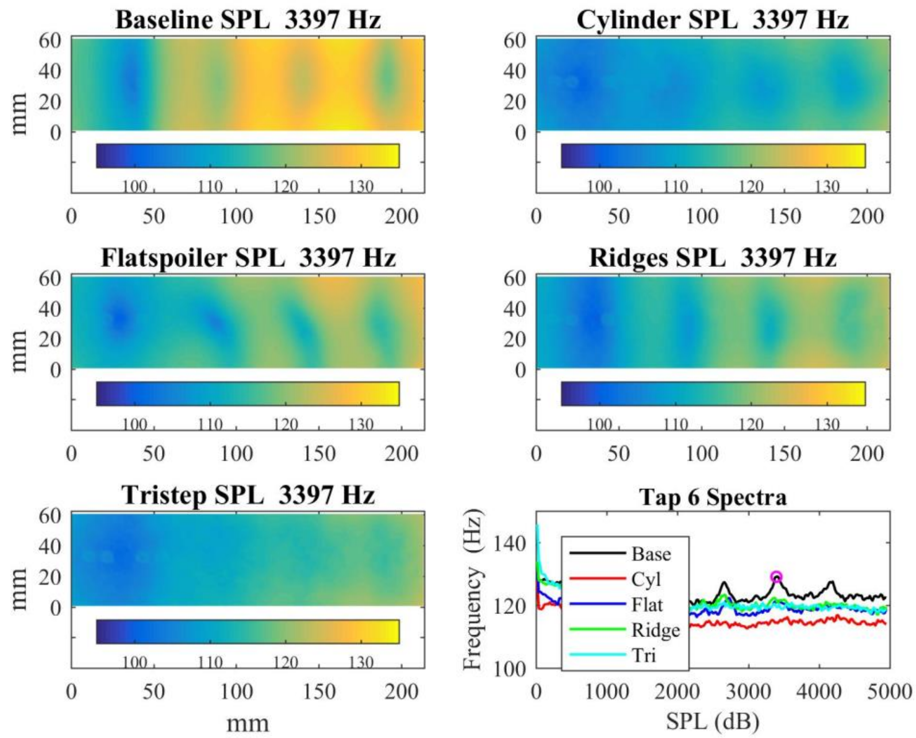

Figure 11. SPL contours for baseline and all control cases at M = 1.5 for the 5th Rossiter tone.

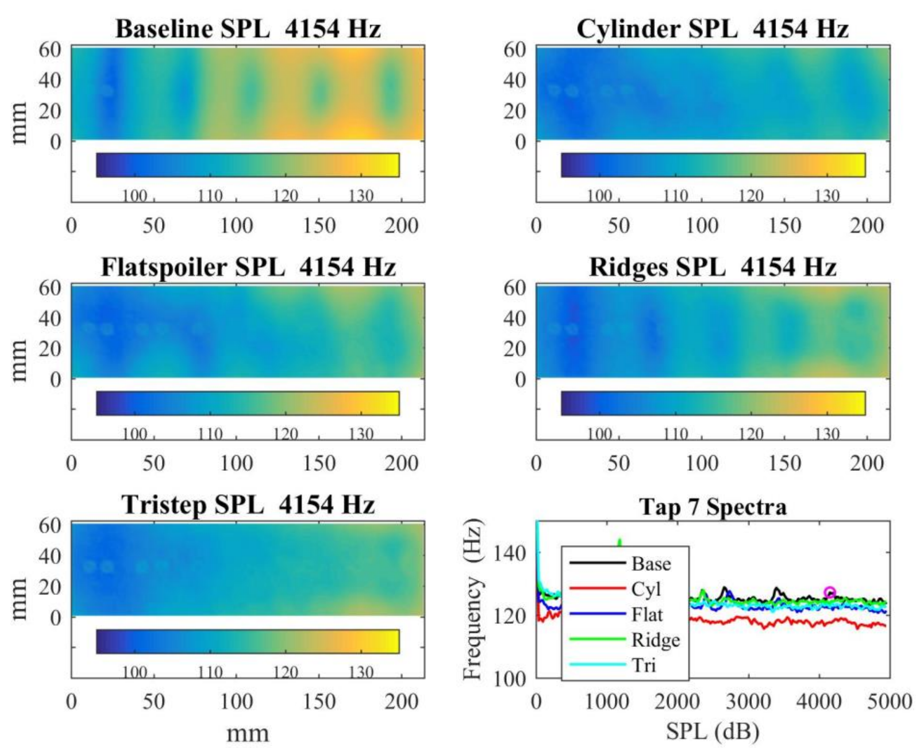

Figure 12. SPL contours for baseline and all control cases at M = 1.5 for the 6th Rossiter tone.

Further insight into the flow may be gained by inspecting the POD modes. Modes 7 through 9 and mode 11 indicate that there is an asymmetric structure on the back part of the cavity. This structure is similar to the asymmetric distribution that is evident in the cavity with the flat spoiler and rod in cross flow control devices (Figure 8 - Figure 12). The presence of this weak asymmetric mode in the baseline cavity suggests that these flow control devices are not creating the asymmetric flow, but enhancing a fluid structure that is already present in the cavity. It is possible that this asymmetric structure may be related to a slight misalignment of the model with the tunnel flow. In any case, the presence of this asymmetric mode in the baseline cavity is impossible to detect without the POD modes as the energy in modes 7-11 is about 1% per mode.

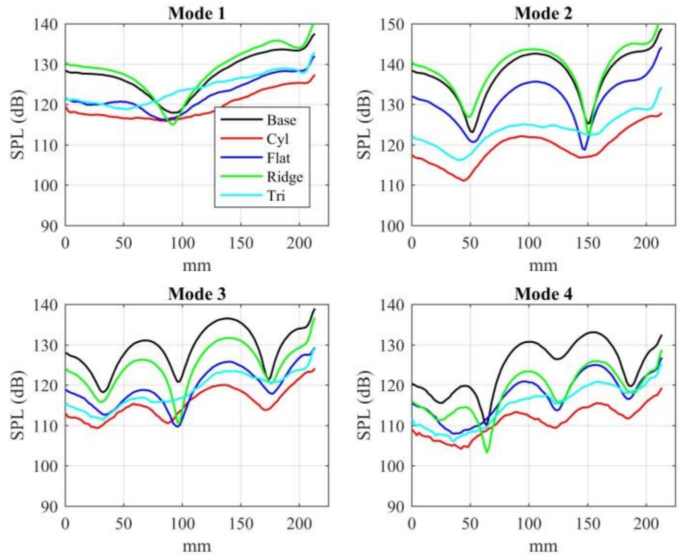

Figure 13. Spanwise SPL profiles at y = 14 mm and M = 1.5 for (a) 1st Rossiter mode, (b) 2nd Rossiter mode, (c) 3rd Rossiter mode, and (d) 4th

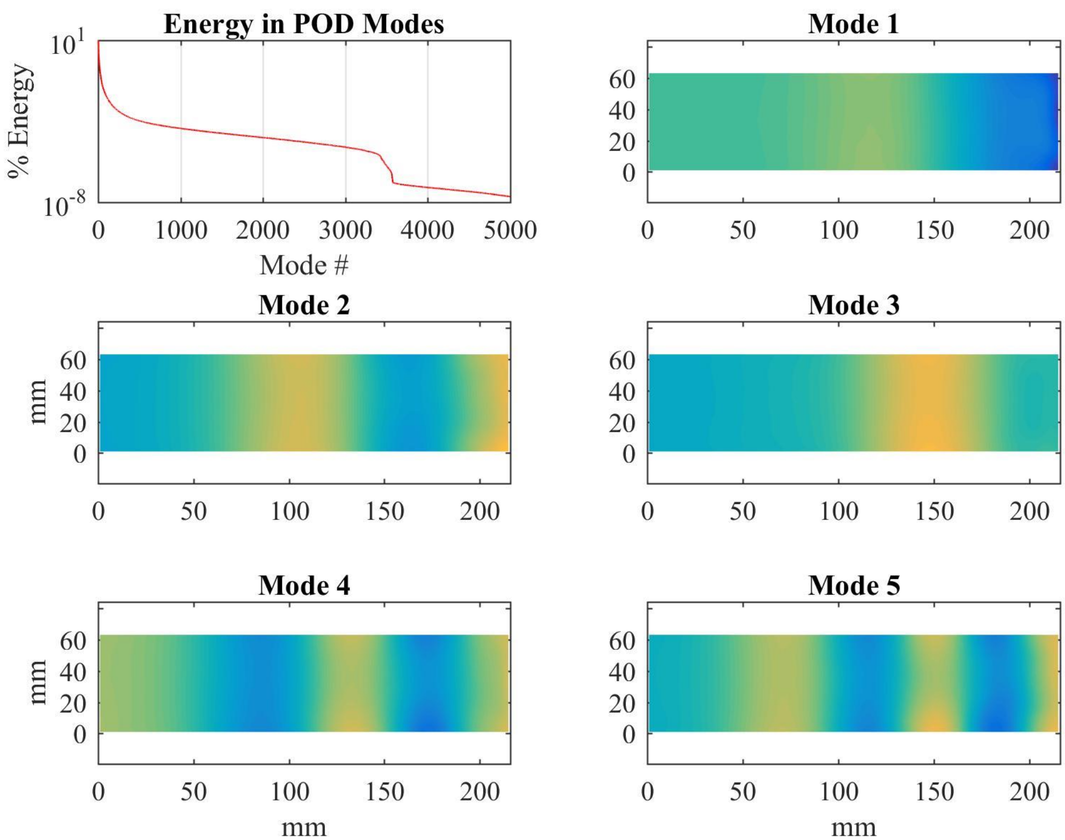

Figure 14. POD Mode energy distribution and first five modes for the baseline cavity at Mach 1.5.

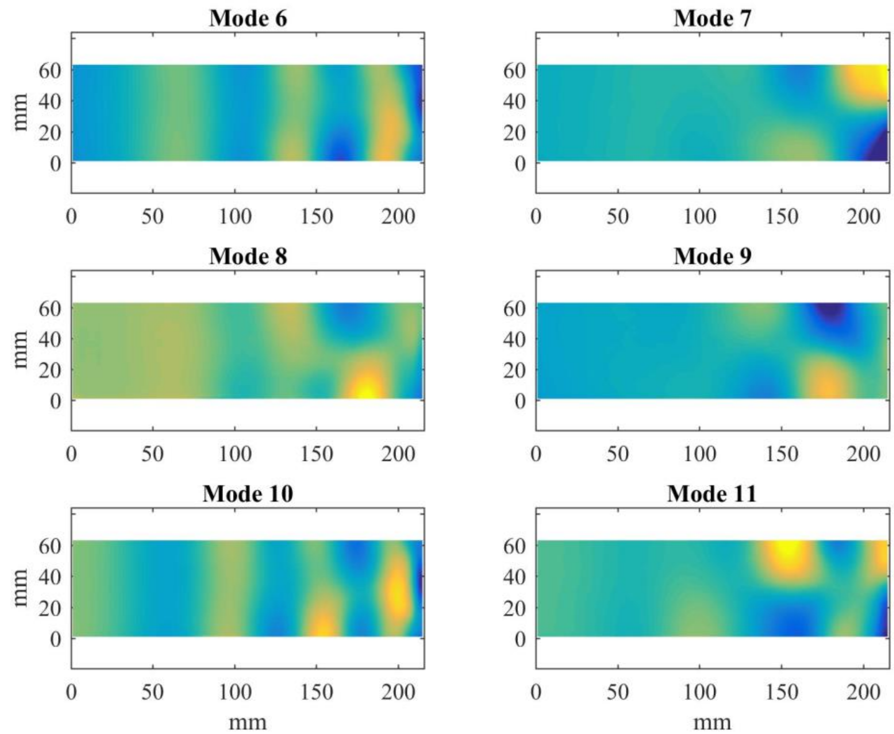

Figure 15. POD modes 6 - 11 for the baseline cavity at Mach 1.5.

D. Subsonic Cavity

A total of 30,000 images were acquired at the five test configurations (baseline plus four flow control setups) at Mach 0.7. The sample rate for the PSP data at Mach 0.7 was 10,000 Hz. Wind-off and background data was also acquired at each test condition and the data was processed and mapped onto the 108 by 32 mesh as described previously. Data was also acquired from the seven Endevco pressure transducers mounted flush with the cavity ceiling along the length of the centerline. Data was acquired from the pressure transducers at 75-khz at each test condition, again, the data was not synchronized with the PSP data acquisition.

The PSP data was extracted at each pressure tap location and the spectral content of the PSP data was computed. The resulting PSP spectra is compared to the tap data at four locations for the baseline and cylinder in cross flow cases in Figure 16. The PSP data is in good agreement with the Endevco measurements. The PSP captures the same Rossiter tone frequencies as the Endevco

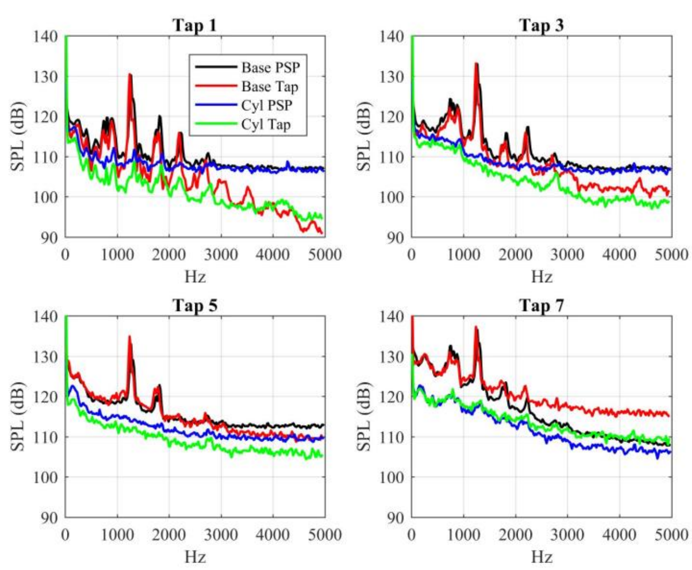

Figure 16: Comparison of PSP and Endevco spectra at 4 locations for baseline and cylinder configurations at M = 0.7.

transducers. The peak amplitudes are within 4.5 dB for the first four tones. At the higher frequencies, it appears that the PSP data has reached a noise floor and is unable to resolve the pressure fluctuations. This is particularly evident at tap 1. Finally, it is again noted that the peak frequencies from this entry do vary slightly from the side wall entry and these are compared in Table 2.

The distribution of SPL over the cavity ceiling at each Rossiter tone for the baseline configuration is shown in Figure 17. There is a distinct spatial dependence on the Rossiter tones and as noted previously the PSP could only resolve modes one through four. The pressure fluctuations manifest as symmetric bands on the cavity ceiling. The SPL distributions for each flow control device at the observed Rossiter tone peaks for the Mach 0.7 cavity are shown in Figure 18 - Figure 21. As in the supersonic case, the rod in cross flow provides the most effective noise suppression. The flat spoiler, which performed poorly in the supersonic case, performs quite well in the subsonic test. The large triangular step performance is slightly below that of the rod and flat spoiler. The ridges do an extremely poor job of noise suppression in the subsonic test.

Table 2: Peak Rossiter frequencies from the side wall and ceiling tests at Mach 0.7.

Mode	Side Wall (Hz)	Ceiling (Hz)
1	796	820
2	1254	1250
3	1748	1797
4	2224	2227

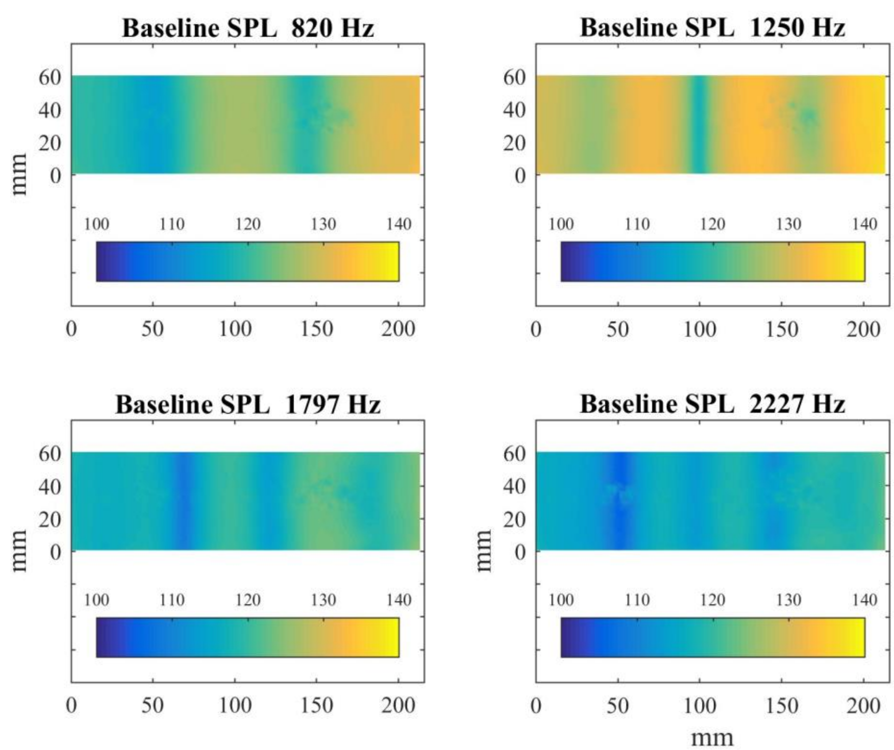

Figure 17: SPL distribution at first four Rossiter tones for M = 0.7 baseline configuration.

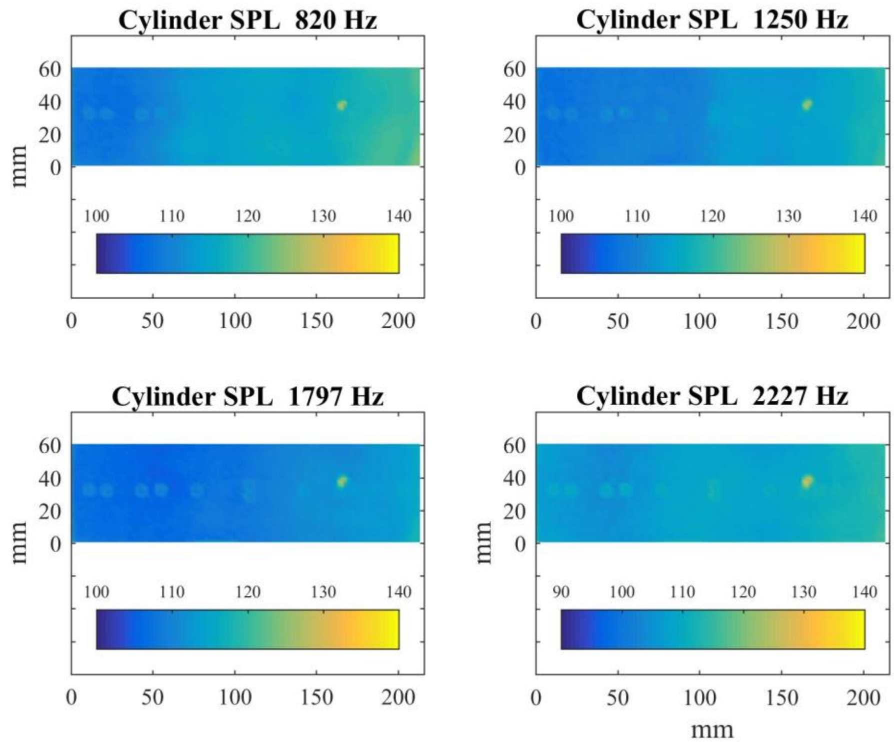

Figure 18: SPL distribution at first four Rossiter tones for M = 0.7 cylinder in cross flow configuration.

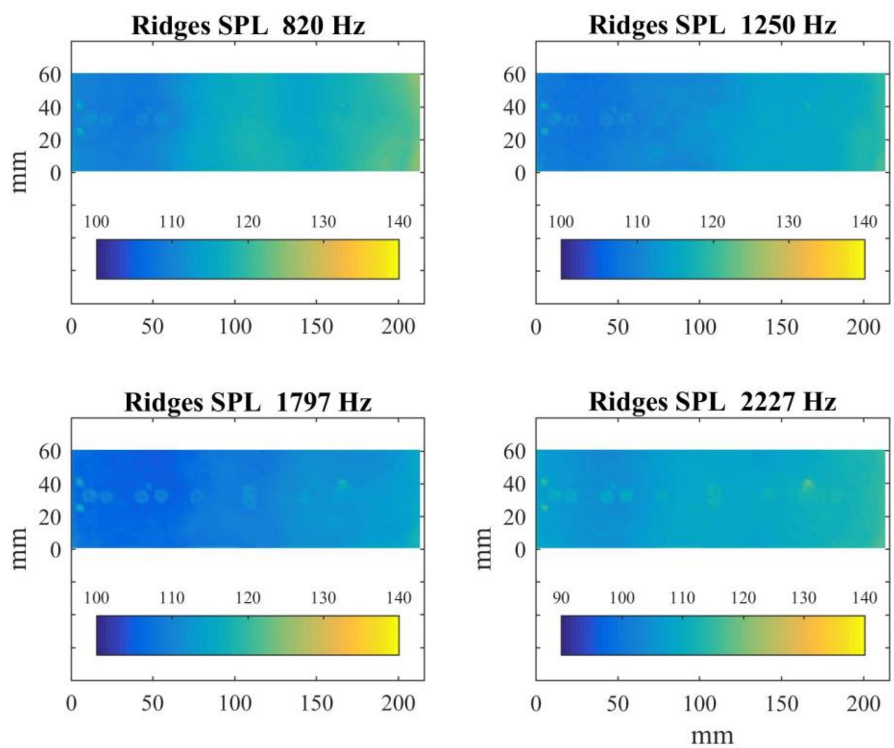

Figure 19: SPL distribution at first four Rossiter tones for M = 0.7 ridges configuration.

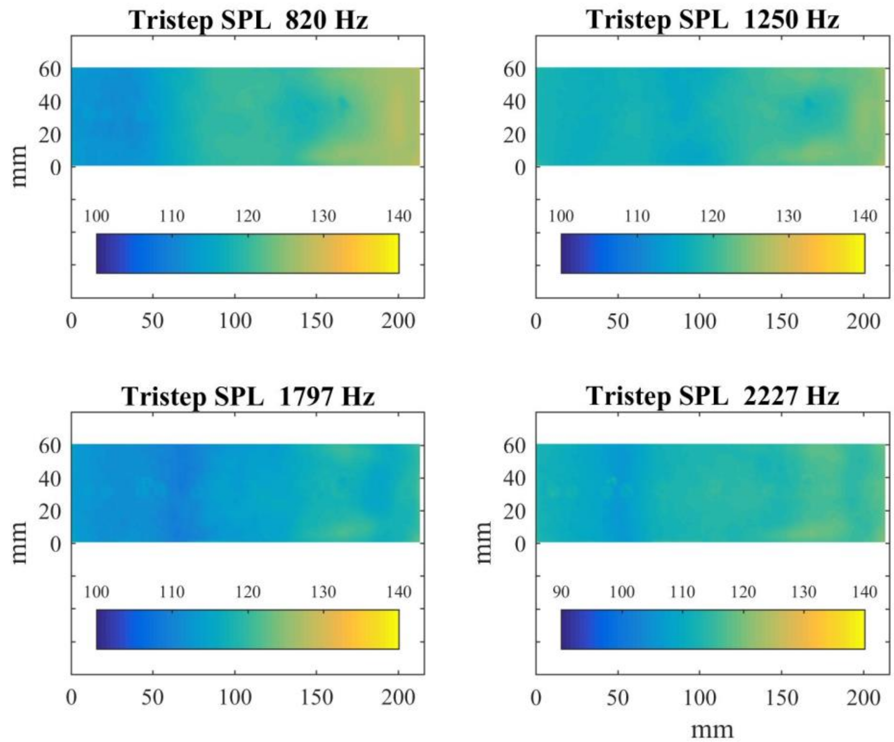

Figure 20: SPL distribution at first four Rossiter tones for M = 0.7 tristep configuration.

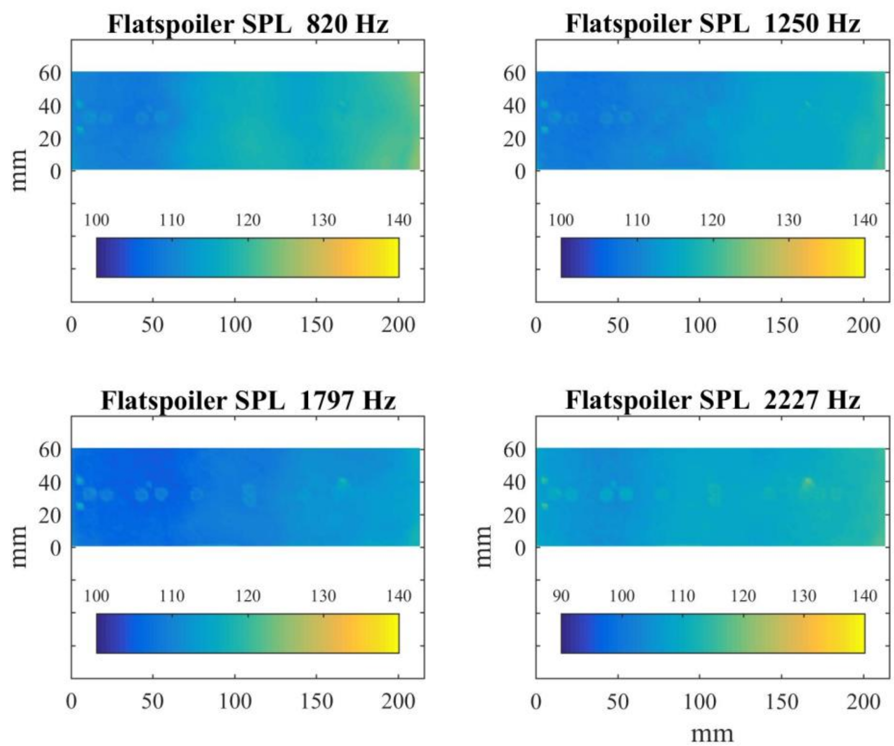

Figure 21: SPL distribution at first four Rossiter tones for M = 0.7 flat-spoiler configuration.

IV.Conclusions and Future Work

In this study, a fast-response pressure sensitive paint was used to take novel, full-field measurements of SPL on the ceiling of a cavity at both subsonic and supersonic conditions. The spectral content and overall sound pressure level measured with the PSP compared well with data taken with the Endevco pressure transducers. The results of the PSP study confirmed previous findings from passive flow control studies at Mach 0.7, namely, that the rod in cross flow, large triangular step, and flat spoiler all serve to suppress the amplitude of the Rossiter tones, while ridges have little to no effect. The high-resolution afforded by the PSP also showed that the regular spatial fluctuations observed in the no-control and ridges cases were disrupted by the other three flow control devices. For the Mach 1.5 case, the cylinder in cross-flow, and to a lesser degree, the tri-step flow control devices suppressed the amplitude of the Rossiter tones while the ridges device had little impact. The flat-spoiler introduced a strong cross-flow mode that is not evident in the baseline data. Analysis of the PSP data using POD revealed several POD modes with spatial profiles very similar to the Rossiter tones, as expected. Other POD modes contained significant content that is believed to be related to model vibrations and camera noise. Finally, POD analysis indicates that there is a weak asymmetric mode in the baseline data that is similar to the strong asymmetric mode evident in the flat-spoiler data. It is suggested that the flat-spoil device is enhancing this mode rather than creating it. This mode may be a result of a slight misalignment of the cavity with the free-stream flow. These spatial fluctuations in SPL were only visible due to the high resolution of the PSP system.

References

[1] LN Cattafesta, DR Williams, CW Rowley, and FS Alvi, "Review of Active Control of Flow-Induced Cavity Resonance," AIAA Paper 2003-3567, (2003).

[2] R Murray and G Elliott, "Characteristics of the Compressible Shear Layer over a Cavity," *AIAA Journal*, Vol. 39, pp. 846-856, 2001

[3] T Liu and JP Sullivan, Pressure and Temperature Sensitive Paints, Springer-Verlag, Berlin, 2005

[4] JW Gregory, H Sakaue, T Liu, JP. Sullivan "Fast Pressure-Sensitive Paint for Flow and Acoustic Diagnostics", *Annual Review of Fluid Mechanics*, Vol. 46, pp. 303-330, 2014

[5] Marvin Sellers, Michael Nelson, Jim W. Crafton, "Dynamic Pressure-Sensitive Paint Demonstration in AEDC Propulsion Wind Tunnel 16T", AIAA-2016-1146

[6] W, Flaherty, TM Reedy, GS Elliott, JM Austin, RF Schmit, J Crafton, "Investigation of cavity flow using fast-response pressure-sensitive paint," *AIAA Journal*, Vol. 52, pp. 2462-2470, 2011

[7] S. Michael Spottswood, Timothy J. Beberniss, and Thomas G. Eason, "Full-Field, Dynamic Pressure and Displacement Measurements of a Panel Excited by Shock Boundary-Layer Interaction," AIAA-2013-1016

[8] J Crafton, A Forlines, S Pallucconi, KY Hsu, C Carter, and M Gruber, "Investigation of Transverse Jet Injections in a Supersonic Crossflow Using Fast Responding Pressure-Sensitive Paint," *Exp Fluids*, Vol. 56, 2014

[9] RF Schmit, F Semmelmayer, M Haverkamp, and JE Grove, "Fourier Analysis of High Speed Shadowgraph Images around a Mach 1.5 Cavity Flowfield," AIAA Paper 2011-3961, 2011

[10] RF Schmit, C, McGaha, J Tekell, JG Grove, and M Stanek, "Performrmance Results for the Optical Turbulence Reduction Cavity," AIAA Paper 2009-702, 2009

[11] RF Schmit, F Semmelmayer, M Haverkamp, JE Grove, and A Ahmed, "Analysis of Cavity Pressure Flow Control Using High Speed," AIAA Paper 2012-0738, 2012

[12] JW Gregory, K Asai, M Kameda, T Liu, and JP Sullivan, "A Review of Pressure-Sensitive Paint for High Speed and Unsteady Aerodynamics," Proceedings of the Institution of Mechanical Engineers, Part G, Journal of Aerospace Engineering, Vol. 222, No. 2, pp. 249-290, 2008

[13] VE Mosharov, VN Radchenko, SD Fonov, "Lumenescent Pressure Sensors in Aerodynamics" Central Aerodynamic Institute (TsAGI), Moscow, 1998

[14] W Ruyten, M Sellers, "On-Line Processing of Pressure-Sensitive Paint Images", Journal of Aerospace Computing, Information, and Communication, Vol. 1 no. 9 pp 372-382, 2004

[15] R Engler, U Fey, U Henne, C Klein, W Sachs, "Quantitative Wind Tunnel Studies Using Pressure- and Temperature Sensitive Paints", Journal of Visualization, Vol. 8, pp. 277-284, 2005

[16] E Vardaki, N Stokes, SD Fonov, J Crafton, "Pressure Sensitive Paint Measurements at the ARA Transonic Wind Tunnel", AIAA-2010-4796

[17] A Scroggin, EB Slamovich, JW Crafton, N Lachendro, JP and Sullivan, "Porous polymer/ceramic composites for luminescence-based temperature and pressure measurement", Proceedings of the Materials Research Society Symposium, 1999, vol. 560, pp. 347–352

[18] MC Merienne, Y Le Sant, F Lebrun, B Deleglise, D Sonnet, "Transonic Buffeting Investigation using Unsteady Pressure-Sensitive Paint in a Large Wind Tunnel", AIAA-2013-1136

[19] Nakakita, K. Unsteady pressure distribution measurement around 2D-cylinders using pressure-sensitive paint. AIAA Paper 2007 - 3819, 2007

[20] Pastuhoff, M.; Yorita, D.; Asai, K.; Alfredsson, P.H. Enhancing the signal-to-noise ratio of pressure sensitive paint data by singular value decomposition. Measurement Science and Technology 2013, 24, 075301

[21] MY Ali, A Pandey, and JW Gregory, "Dynamic Mode Decomposition of Fast Pressure Sensitive Paint Data", Sensors, Vol. 16, pp. 862, 2016

[22] Marvin Sellers, Michael Nelson, Jim W. Crafton, "Dynamic Pressure-Sensitive Paint Demonstration in AEDC Propulsion Wind Tunnel 16T", AIAA-2016-1146